

# Optical damage limits in chalcogenide nonlinear crystals used in 1064 nm pumped nanosecond optical parametric oscillators

Valentin Petrov,<sup>a)</sup> Georgi Marchev<sup>a)</sup>, Aleksey Tyazhev<sup>a)</sup>, Marina Starikova,<sup>a)</sup> Adolfo Esteban-Martin,<sup>a,b)</sup> Vladimir Panyutin,<sup>a)</sup> Valeriy Badikov,<sup>c)</sup> Galina Shevyrdayeva,<sup>c)</sup> Dmitrii Badikov,<sup>c)</sup> Manuel Reza,<sup>a)</sup> Svetlana Sheina,<sup>c)</sup> Anna Fintisova<sup>c)</sup>

<sup>a)</sup>Max-Born-Institute for Nonlinear Optics and Ultrafast Spectroscopy,  
2A Max-Born-Str., D-12489 Berlin, Germany;

<sup>b)</sup>ICFO-Institut de Ciències Fòniques, Mediterranean Technology Park, 08860 Castelldefels,  
Barcelona, Spain;

<sup>c)</sup>High Technologies Laboratory, Kuban State University, 149 Stavropolskaya Str., 350040  
Krasnodar, Russia

## ABSTRACT

We investigated optical damage (surface and bulk) in wide band-gap (absorption edge below 532 nm) sulphide and selenide nonlinear crystals that can be used in 1064-nm pumped optical parametric oscillators (OPOs) for generation of idler pulses above 4  $\mu\text{m}$  without two-photon absorption losses at the pump wavelength. The optical damage has been characterized at the pump wavelength for different repetition rates. Surface damage has been studied for uncoated and antireflection-coated (mainly with a single layer for pump and signal wavelengths) samples. Optical damage inside the OPO has a lower threshold and represents at present the principal limitation for the achievable output. It is related to peak and not to average intensities and in many of the studied crystals bulk damage in the form of scattering centers occurs before surface damage. Such bulk damage formation is faster at higher repetition rate. Lower repetition rates increase the lifetime of the crystal but do not solve the problem. In the most successful nonlinear crystal (both in terms of output energy and average power), orange-phase  $\text{HgGa}_2\text{S}_4$ , the safe pump intensity in extracavity measurements is below  $100 \text{ MW/cm}^2$  which corresponds to less than  $1 \text{ J/cm}^2$  for the 8 ns pulse duration (both values peak on-axis). In the OPO, however, peak on-axis fluence should not exceed  $0.3 \text{ J/cm}^2$  limited by the formation of bulk scattering centers. The damage resistivity of yellow-phase  $\text{HgGa}_2\text{S}_4$  or Cd-doped  $\text{HgGa}_2\text{S}_4$  is higher and of the almost colorless  $\text{CdGa}_2\text{S}_4$  it is roughly two times higher but the latter has no sufficient birefringence for phase-matching.

Key words: chalcogenide nonlinear crystals, optical damage, optical parametric oscillators.

## 1. INTRODUCTION

The mid-IR spectral range (3-15  $\mu\text{m}$ ) represents a very wide „gap“, where only few gas but no solid-state lasers (SSLs) have been developed. Indeed, the upper limit of practical SSLs, such as  $\text{Er}^{3+}$  or  $\text{Cr}^{2+}$ , extends to about 3  $\mu\text{m}$ . Other transitions at longer wavelengths exist but temperature quenching of the mid-IR fluorescence ( $\text{Fe}^{2+}$ ) or the lack of suitable pump sources represent basic limitations. In most cases operation at low temperature and/or using pulsed pumping (e.g. for  $\text{Dy}^{3+}$ ) is required. Notwithstanding the recent progress in transition-metal mid-IR lasers, at present the main approach to cover the mid-IR spectral range on the basis of all-SSL technology is down-conversion employing nonlinear crystals (NLCs). There are oxide crystals that are partially transparent in the mid-IR but not more than 4-5  $\mu\text{m}$ . Indeed, the performance of oxide based crystals is affected by multiphonon absorption starting in the best case from about 4  $\mu\text{m}$  and thus non-oxide materials have to be used, such as unary, binary, ternary and quaternary arsenides, phosphides, sulphides, selenides or tellurides. Some of these inorganic crystals transmit up to 20-30  $\mu\text{m}$  before multiphonon absorption occurs as an intrinsic limit. In contrast with the oxides, which can be grown by well mastered and harmless hydrothermal, flux or Czochralski methods, the more complex Bridgman-Stockbarger growth technique in

sealed (high atmosphere) ampoules, with volatile and chemically reactive starting components, is the only method used to produce large size single domain non-oxide crystals, and this certainly hampered their development all the more that special post-growth treatments are needed to restore stoichiometry and improve their optical quality. As a matter of fact such materials exhibit more defects and the residual losses (absorption and scatter) are more than one order of magnitude larger than in the best oxide crystals.

The longer the mid-IR transmission limit the smaller the band-gap of such non-oxide materials which means that down-conversion will require laser pump sources operating at longer wavelengths, or if such do not exist, cascaded schemes based on oxides in the first stage. Efficient frequency conversion is, however, only possible using pulsed laser sources (femtosecond to nanosecond) and most of the chalcogenide mid-IR crystals will suffer two-photon absorption (TPA) at a pump wavelength of 1064 nm (Nd:YAG) because of their low band-gap. Of the non-oxide NLCs with a band-gap corresponding to  $\leq 532$  nm, many exhibit additional limitations related to residual absorption, birefringence, effective nonlinearity, thermal conductivity, or to the growth, availability and some opto-mechanical properties. Operation in the nanosecond regime in optical parametric oscillators (OPOs) is free of restrictions originating from the spectral acceptance or higher order nonlinear effects and has the best potential for achieving high average power and single pulse energy. Notwithstanding the recent rapid development of Tm/Ho ns laser systems at  $\sim 2$   $\mu\text{m}$ , Nd and Yb based systems in the 1- $\mu\text{m}$  spectral range remain the most powerful and scalable pump sources. Such ns OPOs have been demonstrated, however, only with few non-oxide compounds, whose relevant properties are summarized in Table 1. For comparison, the phase-matching angles and the effective nonlinearity are estimated for a chosen idler wavelength of 6.45  $\mu\text{m}$ .

Table 1. Compilation of important properties of nonlinear crystals for which OPO operation with  $\sim 1$   $\mu\text{m}$  pump has been demonstrated. The effective nonlinear coefficients  $d_{\text{eff}}$  (column 3) are calculated at the corresponding phase-matching angle  $\theta$  or  $\varphi$  (column 2), the nonlinear tensor components,  $d_{ij}$ , used for this calculation were derived from the literature (column 6) applying Miller's rule (column 7). The wavelength  $\lambda_F$  (fundamental) at which the nonlinear coefficients have been estimated by SHG is also included in column 6.

Crystal Point group Plane	$\theta / \varphi$ [°] (Interaction)	$d_{\text{eff}}$ [pm/V]	Thermal conductivity [W/mK]	Band- gap $E_g$ [eV]	Miller's $\delta$ [pm/V] or $d_i$ [pm/V] @ $\lambda_F$ for SHG	+ Miller's correction [pm/V]	
AgGaS <sub>2</sub> $\bar{4}2m$	40.50 (oo-e) 45.53 (eo-e)	8.86 13.65	1.4 // $\mathbf{c}$ 1.5 $\perp$ $\mathbf{c}$	2.70	$\delta_{36}=0.12$	$d_{36}=13.65$	
HgGa <sub>2</sub> S <sub>4</sub> $\bar{4}$	45.87 (oo-e) 51.21 (eo-e)	15.57 21.18	2.49-2.85 // $\mathbf{c}$ 2.36-2.31 $\perp$ $\mathbf{c}$	2.79	$d_{36}=27.2$ 1064 nm	$d_{36}=24.56$	
Cd <sub>x</sub> Hg <sub>1-x</sub> Ga <sub>2</sub> S <sub>4</sub> ( $\theta=90^\circ$ , $x=0.55$ ) $\bar{4}$	90.00 (oo-e)	24.94	1.8-1.92 // $\mathbf{c}$ 1.62-1.81 $\perp$ $\mathbf{c}$ ( $x=0.27-0.3$ )	3.22 ( $x=0.55$ )	$d_{36}=27.2$ @ 1064 nm	$d_{36}=24.94$	
LiGaS <sub>2</sub> $mm2$	xz xy	47.77 (oo-e) 40.36 (eo-e)	4.23 5.50	NA	3.76	$d_{31}=5.8$ $d_{24}=5.1$ @ 2300 nm	$d_{31}=5.71$ $d_{24}=5.21$
LiInSe <sub>2</sub> $mm2$	xz xy	36.97 (oo-e) 41.62 (eo-e)	7.26 10.57	4.7-4.5 // $\mathbf{x}$ 4.7-4.8 // $\mathbf{y}$ 5.5-5.8 // $\mathbf{z}$	2.86	$d_{31}=11.78$ $d_{24}=8.17$ @ 2300 nm	$d_{31}=12.08$ $d_{24}=8.65$
BaGa <sub>4</sub> S <sub>7</sub> $mm2$	xz	12.87 (oo-e)	4.94	NA	3.54	$d_{31}=5.1$ @ 2260 nm	$d_{31}=5.07$
CdSiP <sub>2</sub> $\bar{4}2m$	80.46 (oo-e)	90.99	13.6	2.2-2.45	$d_{36}=84.5$ @ 4.56 $\mu\text{m}$	$d_{36}=92.27$	
Ag <sub>3</sub> AsS <sub>3</sub> $3m$	22.04 (oo-e) 24.01 (eo-e) 65.63 (oe-e)	22.89 16.44 3.35	0.113 // $\mathbf{c}$ , 0.092 $\perp$ $\mathbf{c}$	2.2	$d_{31}=10.4$ $d_{22}=16.6$ @ 10.6 $\mu\text{m}$	$d_{31}=12.34$ $d_{22}=19.70$	

These NLCs include Ag<sub>3</sub>AsS<sub>3</sub> (proustite), AgGaS<sub>2</sub> (AGS), HgGa<sub>2</sub>S<sub>4</sub> (HGS), LiInSe<sub>2</sub> (LISe), LiGaS<sub>2</sub> (LGS), BaGa<sub>4</sub>S<sub>7</sub> (BGS), CdSiP<sub>2</sub> (CSP), and the solid solution Cd<sub>x</sub>Hg<sub>1-x</sub>Ga<sub>2</sub>S<sub>4</sub>. Of them only AGS is commercially available while HGS and LISe can be obtained from some laboratories. Table 2 summarizes the OPO characteristics. Idler wavelengths  $>5$   $\mu\text{m}$  (the limit of oxides) have been demonstrated only in few cases [3,6-10,14,17,18,20-28]. The longest wavelength of 11.3  $\mu\text{m}$  has been reached with AGS [7] and the highest energy above 5  $\mu\text{m}$ , equal to 3 mJ, with HGS at 6.3  $\mu\text{m}$  [17]. HGS delivered so far the highest overall energy and average power, 6.1 mJ and 0.61 W, respectively, at 4.03  $\mu\text{m}$  [15].

Table 2. Nanosecond OPOs based on non-oxide crystals pumped by Nd-lasers. SR: singly resonant, DR: doubly resonant, ND: near degeneracy, SF: single frequency, SP: single pump pass, DP: double pump pass, TT: temperature tuning, NCPM: non-critical phase-matching, RISTRA: Rotated Image Singly-Resonant Twisted RectAngle, NA: not available.

Crystal-type, cut angle	Length [mm]	Pump parameters: $\lambda_p$ , $T_p$ , Rep. rate, Mode	Idler tuning range [ $\mu\text{m}$ ]	Idler energy	[Ref.]
Ag <sub>3</sub> AsS <sub>3</sub> -I, 30°	3.8	1064 nm, 200 ns, 2 kHz, SP, TEM <sub>00</sub>	ND, DR	NA	[1]
Ag <sub>3</sub> AsS <sub>3</sub> -I, 29.5°* see [3]	10	1065 nm, 26 ns, 2 Hz, SP, TEM <sub>00</sub> , SF	2.13-2.56, DR	>10 $\mu\text{J}$	[2]
Ag <sub>3</sub> AsS <sub>3</sub> -I, 28°	10	1065 nm, 25 ns, 2 Hz, SP, TEM <sub>00</sub>	2.13-8.5, SR	<2.5 $\mu\text{J}$ @ 4.5 $\mu\text{m}$	[3]
AGS-I, 50.5°	20	1064 nm, 20 ns, 10 Hz, SP, TEM <sub>00</sub>	2.128-4, SR	250 $\mu\text{J}$ @ 2.128 $\mu\text{m}$	[4]
AGS-I, 49°	20	1064 nm, 10.9 ns, 10 Hz, DP	2.77-4.2, SR	120 $\mu\text{J}$ @ 3.5 $\mu\text{m}$	[5]
AGS-II, 39.9°	25	1064 nm, 10 ns, 3.3 Hz, DP	6.7-9.8, SR	1200 $\mu\text{J}$ @ 8.2 $\mu\text{m}$	[6]
AGS-II, 45.1°	20	1064 nm, 20-30 ns, 10 Hz, DP, TEM <sub>00</sub>	3.9-11.3, SR	372 $\mu\text{J}$ @ 6 $\mu\text{m}$	[7]
AGS-I, 47°	20	1064 nm, 10-30 ns, <10 Hz, DP, TEM <sub>00</sub>	2.6-5.3, SR	620 $\mu\text{J}$ @ 4 $\mu\text{m}$	[8-10]
HGS-II, 67.5°	8	1064 nm, 10 Hz, DP	~3.7-4.5, SR	NA	[11]
HGS-II, 67.5°	8	1064 nm, 5 ns, 30 Hz, DP	4.18-4.438, SR, TT	3.67 mJ @ 4.18 $\mu\text{m}$	[12]
HGS-I, 52°	6	1064 nm, 30 ns, 10 Hz, SP, TEM <sub>00</sub>	2.3-4.4, SR	360 $\mu\text{J}$ @ 2.37 $\mu\text{m}$	[13]
HGS-I, 52.7°	10.1	1064 nm, 4.4 ns, 20 Hz, SP	3.69-5.69, SR	3.3 mJ @ 4.03 $\mu\text{m}$	[14]
HGS-I, 52.7°	13.4	1064 nm, 8 ns, 100 Hz, DP	<3-8, SR	6.1 mJ @ 4.03 $\mu\text{m}$	[15]
HGS-I, 52°	6	1064 nm, 15 ns, 10 Hz, DP, TEM <sub>00</sub>	3.75-4.65, SR, TT	~65 $\mu\text{J}$ @ 4.35 $\mu\text{m}$	[16]
HGS-II, 50.2°	10.76	1064 nm, 8 ns, 10 Hz, DP	4.5-9, SR	3 mJ @ 6.3 $\mu\text{m}$	[17]
Cd <sub>x</sub> Hg <sub>1-x</sub> Ga <sub>2</sub> S <sub>4</sub> -I, x=0.21-0.56, 74-90°	10.9-11.6	1064 nm, 22-30 ns, 10 Hz, SP, TEM <sub>00</sub>	2.85-8.9, SR, in part NCPM	400 $\mu\text{J}$ @ 3.03 $\mu\text{m}$ 270 $\mu\text{J}$ @ 5.76 $\mu\text{m}$ 110 $\mu\text{J}$ @ 8.9 $\mu\text{m}$	[18]
LISE-II, 72°	17	1064 nm, 10 ns, 10 Hz, DP	3.34-3.82, SR	92 $\mu\text{J}$ @ 3.457 $\mu\text{m}$	[19]
LISE-II, 41.6° LISE-II, 34°	17.6, 24.5	1064 nm, 14 ns, 100 Hz, DP	4.65-7.5, SR 5.45-8.7, SR	282 $\mu\text{J}$ @ 6.5 $\mu\text{m}$ 116 $\mu\text{J}$ @ 8.4 $\mu\text{m}$	[20-22]
CSP-I, 90°	8	1064 nm, 14 ns, 10-20 Hz, DP	6.2, SR, NCPM	470 $\mu\text{J}$ @ 6.2 $\mu\text{m}$	[23]
CSP-I, 90°	9.5	1064 nm, 1 ns, 1 kHz, DP	6.117-6.554, SR, NCPM, TT	24 $\mu\text{J}$ @ 6.125 $\mu\text{m}$	[24]
CSP-I, 90°	7	1064 nm, 0.4 ns, 1-10 kHz, DP, TEM <sub>00</sub> , SF	6.15, SR	4.3 $\mu\text{J}$ @ 6.15 $\mu\text{m}$	[25]
CSP-I, 90°	9.5	1064 nm, 14 ns, 100 Hz, SP	6.125, RISTRA	64 $\mu\text{J}$ @ 6.125 $\mu\text{m}$	[26]
LGS-II, 40.6°	8	1064 nm, 8 ns, 100 Hz, DP	5.46, SR	134 $\mu\text{J}$ @ 5.46 $\mu\text{m}$	[27]
LGS-II, 40.6°	8.2	1064 nm, 1 ns, 1 kHz, DP	4.046-6.014, SR	1.1 $\mu\text{J}$ @ 5.46 $\mu\text{m}$	[27]
BGS-I, 9.2°	14.05	1064 nm, 8 ns, 100 Hz, DP	5.5-7.3, SR	500 $\mu\text{J}$ @ 6.217 $\mu\text{m}$	[28]

Although major progress has been achieved with such OPOs starting from 2005, after we introduced LISe, LGS, CSP, BGS, and Cd<sub>x</sub>Hg<sub>1-x</sub>Ga<sub>2</sub>S<sub>4</sub> as new promising mid-IR NLCs, it can be easily seen from Table 2 that the present state-of-the-art is still quite restricted with respect to all essential output characteristics: idler wavelength, energy, repetition rate and average power. If the reasons shall be summarized in a single statement it could read: insufficient parametric gain to reach few times above threshold damage-free operation or low slope efficiency, especially away from degeneracy. Crystal length can greatly reduce OPO threshold but it is limited not only from high optical quality growth considerations (max. 25 mm in Table 1) but also because residual losses in the clear transparency range are rather high in some crystals like CSP or LISe.

The effective nonlinear coefficient is of course of primary importance to reduce the OPO threshold, too. There exist, however, some fundamental relations between the nonlinearity and the index of refraction. Although the nonlinear

coefficients  $d_{ii}$  may vary a lot, the quantity  $\delta = d_{ii}/(n^2-1)^3 = d_{ii}/(\chi^{(1)}-1)^3$  (Miller's delta) remains almost constant (e.g. within one order of magnitude, Miller's empirical rule). Mid-IR NLCs have  $n > 2$  and empirical formulae indicate that the index of refraction depends on the material band-gap as  $\sim E_g^{-1/4}$  [29], hence, at  $n \gg 1$ ,  $d \sim E_g^{-3/2}$  (here  $d$  is some average nonlinearity). The index of refraction also enters the expression for the coupling constant in three-photon parametric interaction equations and it is not the  $d$ -tensor that should be compared for different materials but rather some figure of merit, such as  $FM \sim d^2/n^3$ , which determines the conversion efficiency. Thus, at  $n \gg 1$ , one obtains  $FM \sim n^9 \sim E_g^{-9/4}$  [29]. When comparing operation at different wavelengths one should have in mind that besides the weak dependence (dispersion) of the  $d_{ii}$  tensor components, which can be estimated from Miller's rule on the basis of the refractive index dispersion, there is much stronger dependence through the coupling constant and the figure of merit can be redefined as  $FM^* \sim d^2/(n^3 \lambda_1 \lambda_2 \lambda_3)$ . Thus, operation at longer (idler) wavelengths away from degeneracy in general means higher OPO threshold and lower conversion efficiency, which is a fundamental limitation at a fixed pump wavelength.

Although the number of cavity round-trips is smaller, the OPO threshold in terms of pump fluence is lower with shorter pump pulses. This can be seen from Table 2 where pump durations not exceeding 30 ns have been exclusively employed in Nd-laser pumped OPOs, with one exception, the very first  $Ag_3AsS_3$ -based OPO in which surface damage occurred within minutes [1]. This can be understood on the basis of higher optical damage intensity limit when the pulses get shorter, although this increase is slower compared to the pulse peak intensity dependence, i.e. the optical damage threshold depends both on pump fluence and on intensity. Another serious limitation is evident from Table 2 also with respect to the repetition rate. It is related to a lesser extent to thermal effects like lensing or phase-mismatch caused by local heating as a consequence of residual crystal absorption than to a "cumulative" damage at higher repetition rates. Thus, most such OPOs were operated at 10 Hz, in rare cases at 100 Hz, and damage-free operation at kilohertz repetition rates has only been achieved with pump pulse durations of 1 ns or less [24,25,27].

The above makes it clear how detrimental damage effects in mid-IR NLCs are when such crystals are employed in ns OPOs. In fact this is the main reason why such devices pumped near 1  $\mu m$  never became commercially available. In Sections 4-6, we present some of our observations on optical damage (surface and bulk) effects in two families of wide band-gap chalcogenide NLCs used in 1064-nm pumped OPOs for generation of idler pulses above 4  $\mu m$ . We select two extremes from Table 1: HGS is the crystal with one of the highest FM that delivered the highest OPO output so far. BGS is a crystal with one of the lowest nonlinear FM but one of the largest band-gaps for which still the OPO threshold could be reached. There is a selenide analogue of BGS,  $BaGa_4Se_7$  (BGSe) with higher nonlinearity / smaller band-gap, but there is no selenide analogue of HGS that has been successfully grown in large size. Instead, doping of HGS with Cd ( $Cd_xHg_{1-x}Ga_2S_4$ ) can be used to improve some of its properties, including damage resistivity and growth habit. The optical damage has been characterized in the present study at 1064 nm, for different repetition rates and pulse durations, extracavity and inside the OPO.

## 2. OPTICAL DAMAGE IN MID-IR OPOs: PREVIOUS OBSERVATIONS

In the literature one finds some systematic optical damage studies on specific NLCs, e.g.  $ZnGeP_2$ , but no systematic study of such mid-IR NLCs that can be pumped near 1  $\mu m$ . There exists only one comparative study with 30-ns long pulses but it is at a wavelength of 9.55  $\mu m$  related to  $CO_2$  laser frequency doubling [30]. While this study indeed offers the opportunity to compare many NLCs without TPA effect, it is impossible to conclude that the results are useful at 1064 nm. Still it is interesting that HGS showed the highest surface damage resistivity out of 9 NLCs in this study ( $\sim 300$  MW/cm<sup>2</sup> or  $\sim 9$  J/cm<sup>2</sup> peak axial values), roughly two times higher than AGS. As could be expected, far from the band-gap, different phases of HGS (yellow and orange) or doping with Cd ( $Cd_xHg_{1-x}Ga_2S_4$ ) gave similar results.

Therefore, most interesting are direct damage observations in 1- $\mu m$  pumped OPOs. Surface damage of  $Ag_3AsS_3$  (uncoated and AR-coated) was seen in the very first Nd-laser pumped OPO [1] at very low pump intensity (450 kW/cm<sup>2</sup>) although repetition rate, pulse duration and doubly-resonant operation were untypical, see Table 2. Safe operation of the proustite OPO was obtained at  $< 10$  MW/cm<sup>2</sup> peak pump intensity (26 ns pump pulses) at 2 Hz, while surface damage occurred in separate tests after 10 pulses of 20 ns duration with 25 MW/cm<sup>2</sup> [2]. AR coating only slightly improved the damage resistivity. Surface damage of the crystal exit face occurred in the OPO at 19 MW/cm<sup>2</sup> after many pulses (after 1-2 h at 2 Hz) but had little effect on the performance [2]. Finally, singly resonant operation could be achieved with proustite, which did not require single frequency pump source, below its damage threshold of 20 MW/cm<sup>2</sup> at 2 Hz [3]. In this early work one finds the first hint that resonated signal wave contributes to the crystal damage at high output levels.

The surface damage threshold intensity of the first AGS crystal used in such an OPO was not better: 13 MW/cm<sup>2</sup> with 100 and 10 MW/cm<sup>2</sup> with 1000 pulses of 20 ns duration at 10 Hz [4], inside the OPO these limits were lower due to the signal wave and did not permit operation beyond 4 μm, Table 2. Higher damage thresholds (partial surface damage) for AGS in such an OPO were given in [5]: <30 MW/cm<sup>2</sup> for single shot (10 pulses of ~8 ns duration) and ~26 MW/cm<sup>2</sup> at 10 Hz (50 shots of ~11 ns duration). Also in this case, it was surface damage that limited the idler tunability from the long wave side. Surface damage on both AGS surfaces was observed at 30 MW/cm<sup>2</sup> in the OPO pumped with 10 ns pulses at 1064 nm [6] but these authors stated that there could be a lot of room for improvement because of the >500 MW/cm<sup>2</sup> bulk damage limit under the same conditions. At 10 Hz, surface damage of the AR-coated AGS occurred at 0.2 J/cm<sup>2</sup> for 3000 shots (5 min) which translates into only 7-10 MW/cm<sup>2</sup> [7] but outside the OPO cavity the damage threshold was 3 times higher. No surface damage was observed in the AGS OPO in [8-10] up to 34 MW/cm<sup>2</sup> (15 ns duration) but this seems to be at 1 Hz.

Since often authors do not specify if their damage thresholds correspond to average or peak fluence/intensity, relative measurements are sometimes more informative; thus 2 times better damage resistivity of HGS compared to AGS was given in [11]. An absolute value of 60 MW/cm<sup>2</sup> (0.3 J/cm<sup>2</sup>) for AR-coated HGS was measured at 30 Hz for 5-ns long pump pulses at 1064 nm for the same sample [12]. For uncoated HGS, measurements with 30 ns pulses outside the OPO indicate damage threshold between 40 and 60 MW/cm<sup>2</sup> (1.2-1.8 J/cm<sup>2</sup>, basically single shot) at 1064 nm [31] and confirm roughly 2 times better resistivity compared to AGS [11,30]. The surface damage limit we observed in 2-mm thick uncoated orange HGS with 1-ns 1064-nm pulses at 1 kHz was ~400 MW/cm<sup>2</sup> or ~0.4 J/cm<sup>2</sup> (peak values) [31].

In the first CSP OPO experiment damage occurred at ~0.44 J/cm<sup>2</sup> (~31 MW/cm<sup>2</sup> for 14 ns long pulses at 10 Hz), both peak on-axis values [23]. However, no damage occurred to CSP in the 1-ns pulse pumped OPO operating at 1 kHz for similar intensities [24]. In this regime damage threshold (peak) for AR-coated CSP plate was determined extracavity at 0.38 J/cm<sup>2</sup> (380 MW/cm<sup>2</sup>) in 12 s long tests at 500 Hz. With 0.4 ns long pulses we obtained damage free OPO operation up to 145 MW/cm<sup>2</sup> at 1 kHz [25]. Outside the cavity uncoated plates of CSP exhibited surface damage threshold of 0.27 J/cm<sup>2</sup> or 34 MW/cm<sup>2</sup> for 8 ns pulses in 1 min long tests at 100 Hz. It seems AR-coating is capable of slightly improving the surface damage resistivity of CSP. Nevertheless, the relatively low damage thresholds are rather unexpected having in mind the high thermal conductivity (Table 1) so they might be related to more defects in this material which is still in its initial phase of development.

The situation with LISe was more complex mainly related to the reproducibility of the results. For uncoated and AR-coated LISe test plates, complete damage (surface and crack) occurred for 14 ns long pulses at 1064 nm and 100 Hz within seconds/minutes for on-axis fluence of 0.78-0.92 J/cm<sup>2</sup> (56-66 MW/cm<sup>2</sup> peak on-axis pump intensity). In several cases irreversible whitened spots (surface deterioration) were observed starting from an on-axis fluence of 0.5 J/cm<sup>2</sup> or a peak on-axis intensity of 36 MW/cm<sup>2</sup>. This is the minimum fluence value for which such kind of damage was observed, and there is obvious dependence on the position and the sample. The whiter spots appear on uncoated surfaces, however, they occur also on AR-coated surfaces, presumably beneath the layer. In most of the cases they occurred at higher pump energies and in one of the uncoated test plates they did not occur at all, until complete damage was observed which seems to indicate that this effect is related to the polishing/coating procedure since all samples were from the same LISe boule. In principle the AR-coating applied seems to be sufficiently resistant for OPO operation and in some cases the surface damage threshold was higher for the AR-coated surface. But the quality of the coating is not reproducible as evidenced in the OPO experiment [20-22], in which always one of the surfaces (the one with higher residual reflection) got damaged at lower pump levels, independent whether it was a front or rear surface with respect to the pump. The lowest pump level at which surface damage to an OPO LISe sample in the form of whitened spots on the coating (or beneath it), were observed, was a peak on-axial pump intensity of 16 MW/cm<sup>2</sup>. This corresponds to operation roughly two times above the threshold and strong signal field is already present in the cavity. By translating the sample in transversal direction, we observed several times the same kind of damage to the same surface, the one with higher residual reflectivity of the AR-coating, independent of the orientation of the sample with respect to the pump beam (entrance or exit surface). No damage occurred to the other surface of the sample. The same OPO AR-coated LISe sample was studied for damage also extracavity, using the same pump source and fresh positions. The tests were performed for 60 s at 100 Hz. Again the same surface had low damage threshold although it was always an exit surface. The damage threshold for the occurrence of similar whitened spots was 23 MW/cm<sup>2</sup>. Full damage to this surface (coating destroyed and crater appeared) occurred at 45 MW/cm<sup>2</sup>. At this same intensity level, the first whitened spot on the other surface (the one with lower residual reflectivity) was observed. It can be only speculated why damage of the LISe OPO samples in the form of whiter surface spot occurred at much lower pump energy when inside the cavity. Nevertheless, the presence of such spots did not affect the OPO performance until the damage developed further. Complete damage

was also observed at lower levels inside the cavity but could be a consequence of already existing whiter spot. There are two possibilities: either contribution from the resonated signal wave (as reported for other crystals) or simply low quality of this AR-coating. Experiments outside the cavity indicated lower damage of the surface with higher residual reflection, also lower threshold for whitening, so it seems more probable that this surface was simply of lower quality and that is why it got damaged although it was not always the front surface in the OPO. The different damage resistivity of the two surfaces could be attributed to the fact that after AR-coating one of the surfaces, the other one was not repolished. Comparing the results with coated and uncoated LISe surfaces it can be anticipated that, for the present quality of the grown material, optimization of the AR-coating process could permit the safe use of peak on-axis intensities of about  $50 \text{ MW/cm}^2$ . Once the problem with the reproducibility of the AR-coating is solved one can expect substantial improvement of the LISe OPO performance [20-22].

The situation with LGS was quite different: Measurements of uncoated and AR-coated (single layer for pump and signal) LGS indicated damage thresholds roughly 5 times higher than for LISe. In addition, the damage threshold values showed good reproducibility and no drops like in the case of LISe, bulk damage was not observed and there was no dependence on the bulk optical quality or aging. There was also no systematic difference between uncoated and AR-coated surface damage thresholds. Since similar coatings were applied also to LISe, one can conclude that the AR-coating problems in LISe are related to the surface chemical stability and not necessarily to the coating itself. The damage tests with LGS plates were performed extracavity with 14 ns, 100 Hz pulses for 1 min because the low OPO efficiency and intracavity signal power do not permit to conclude about further damage mechanisms. Scattering centers (turbidities) were seen in visible light as a first sign of surface damage. They occurred not necessarily in the center of the pump spot and the actual damage developed from them at higher intensity. The cracks occurred in fact on the next day after the experiments and developed from the damaged front surface. The results in terms of peak on-axis fluence were between  $3.33$  and  $3.84 \text{ J/cm}^2$  for observation of turbidity and  $3.52$  and  $4.70 \text{ J/cm}^2$  for complete damage (surface crater or crack).

### 3. OPTICAL DAMAGE LIMITED PERFORMANCE OF BGS AND HGS OPOs

Let us illustrate in this section the optical damage limited operation of two NLCs, BGS and HGS, in the same two-mirror, singly-resonant, double pump pass OPO cavity that we employed also for other materials. A diode-pumped Q-switched Nd:YAG laser/amplifier system served as a pump, see Fig. 1, with a bandwidth of  $30 \text{ GHz}$  ( $1 \text{ cm}^{-1}$ ) and  $M^2$  factor of  $\sim 1.4$ . The pump beam reached the NLCs after reflection at the ZnSe bending mirror (M2) and passing through the output coupler (OC) which is HT for pump and idler.

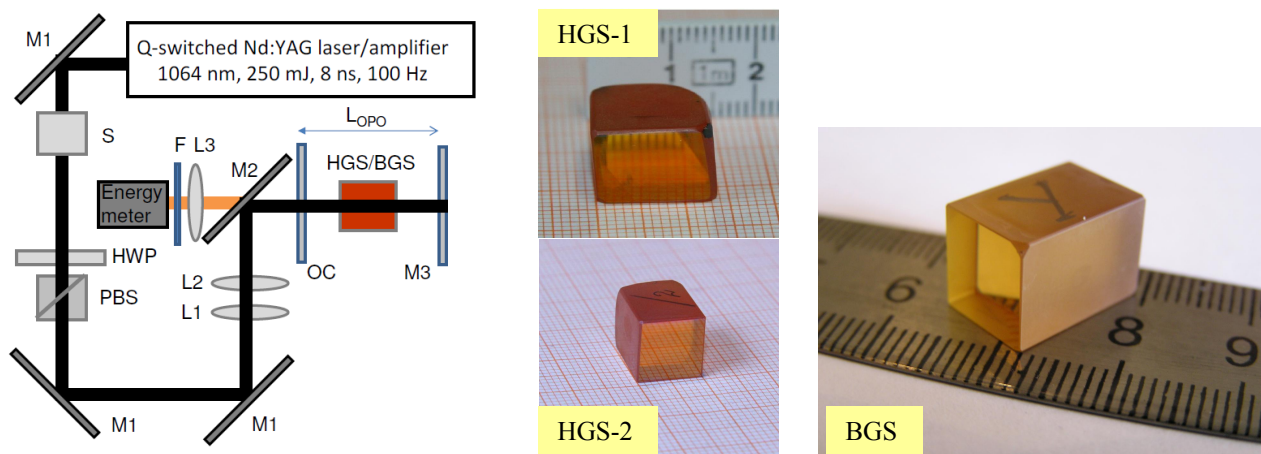


Fig. 1. OPO experimental set-up and active elements used: A mechanical shutter (S) can reduce the repetition rate and the average pump power, a half-wave plate (HWP) and a polarizing beam splitter (PBS) are used as attenuator and a telescope consisting of two lenses L1 and L2 expands the pump beam to a diameter of 9.6 and 8.45 mm (HGS) and  $\sim 5.5$  and  $\sim 8.8$  mm (BGS), in the horizontal and vertical directions, respectively. A plane Ag-mirror acts as a total reflector (M3) for all three waves in a double pump pass singly resonant OPO configuration. The filters (F) suppress the residual pump and signal pulses.

The HGS samples used were a 13.4 mm-long one with an aperture of  $\sim 10 \times 13.6 \text{ mm}^2$  cut at  $\theta=52.7^\circ$  and  $\varphi=45^\circ$  for type-I (oo-e) interaction for the 4- $\mu\text{m}$  range (HGS-1), and a 10.76 mm-long one with an aperture of  $\sim 9.5 \times 9.5 \text{ mm}^2$ , cut at  $\theta=50.2^\circ$  and  $\varphi=0^\circ$  for type-II (eo-e) interaction for the 6.3  $\mu\text{m}$  range (HGS-2), in both cases utilizing only the  $d_{36}$  component of the nonlinear tensor. Effective nonlinearity is  $\sim 36\%$  higher for type-II interaction. The 14.05-mm long BGS element had an aperture of  $9.8 \times 9.5 \text{ mm}^2$ . It was cut in the  $x$ - $z$  plane at  $\theta=9.2^\circ$  for type-I (oo-e) interaction, to ensure maximum effective nonlinearity  $d_{31}\cos\theta \sim d_{31}$ . All three crystals were AR-coated for the resonated signal wavelength which resulted in low residual reflectivity for the pump as well.

For such singly resonant OPO configurations, obviously highest idler extraction can be expected with an OC completely reflecting the signal and transmitting the idler. The main reason to use OCs with partial reflectivity for the signal is to avoid crystal damage at high intracavity signal intensity. Thus, there were some differences in the OC and in the cavity length in the three cases described below. With BGS and HGS-1 a cavity length of 17 mm was employed. The plane-parallel ZnSe OC had a transmission of  $\sim 20\%$  at the signal wave and  $\sim 79\%$  for the idler in the case of BGS, and the wedged ZnSe OC a transmission of 29% at the signal wave and 79% for the idler in the case of HGS-1. The ZnS OC used with HGS-2 had radius-of-curvature of -2 m and transmission of  $\sim 30\%$  for the signal wave and 92% for the idler. In this case the cavity was lengthened to 5.2 cm for better output beam quality. Only the ZnS OC used in the last case had an AR-coating on its rear surface that enabled improved idler extraction.

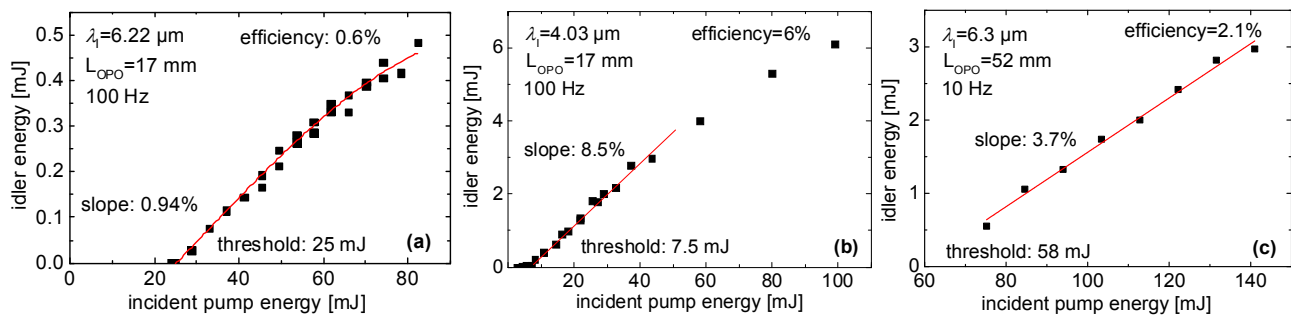


Fig. 2. Input-output OPO characteristics with BGS (a), HGS-1 (b), and HGS-2 (c) with thresholds extrapolated from the idler slope efficiency.

The threshold of 25 mJ with BGS (Fig. 2a) corresponds to an axial fluence of  $0.134 \text{ J/cm}^2$  or a peak on-axis intensity of  $16.7 \text{ MW/cm}^2$ . The threshold of  $\sim 58 \text{ mJ}$  at similar idler wavelength with HGS-2 corresponds to an axial pump fluence of  $0.18 \text{ J/cm}^2$  or a peak intensity of  $\sim 23 \text{ MW/cm}^2$ . This threshold intensity is higher than with BGS although the effective nonlinearity of HGS is superior (Table 1). This can be attributed to the shorter cavity used with BGS, to the different crystal lengths and the better OC feedback (both for signal and idler). The extrapolated threshold with HGS-1 in the 4  $\mu\text{m}$  idler range corresponds to an axial pump fluence of  $22 \text{ mJ/cm}^2$  or a peak intensity of  $\sim 2.7 \text{ MW/cm}^2$ . This is much lower value that can be attributed to the higher parametric gain moving closer to degeneracy, the shorter (compared to HGS-2) cavity length and the longer crystal length.

Although highest idler energies (of any 1- $\mu\text{m}$  pumped non-oxide OPO) were obtained in case (b) of Fig. 2 and damage-free operation far above threshold ( $>10$  times) was possible with this HGS OPO, it is known that highest conversion efficiencies are achieved at lower ratios. The maximum conversion to the idler of  $\sim 7.5\%$  is in fact not at maximum pump level but around 40 mJ which indicates that yet higher output idler energies and average power could be possible if larger apertures of the active element were available. The maximum on-axis intensity applied in this case did not exceed  $40 \text{ MW/cm}^2$ . Of course high conversion efficiency means high intracavity signal power but simultaneously one can expect that the pump is depleted in its maximum.

There is no saturation in the idler energy dependence in case (c) of Fig. 2 due to back conversion because it was impossible to reach a regime 3 times above threshold. The maximum pump level in this case was higher,  $\sim 55 \text{ MW/cm}^2$  axial intensity, although the conversion efficiency was lower. This was, however, safe for the crystal only at lower (10 Hz) repetition rate. Damage developed immediately at 100 Hz at pump levels above 2 times threshold, see Section 5.

At much lower idler power, it is difficult to attribute the slight saturation with BGS in case (a) of Fig. 2 to back conversion. While the origin of this effect is at present unknown, it should be outlined that we suspect here highly

spatially confined operation of the OPO around its axis. This is confirmed by the relatively good  $M^2$  value measured in this case for the idler output ( $\sim 10$ ).  $M^2$  was in the range 180-190 for the two planes in the HGS-1 OPO and improved to  $\sim 30$  with the longer cavity used in the HGS-2 OPO. The highest pump level we applied to the BGS crystal was  $\sim 54 \text{ MW/cm}^2$  axial intensity.

#### 4. OPTICAL DAMAGE OF HGS WITH FOCUSED BEAMS

Depending on the excess HgS in the charge, both yellow and orange phase HGS can be grown.<sup>31</sup> First we studied 4 test plates of HGS which were single-side AR-coated similar to the OPO elements. Two of them (#1 and #3) were orange phase and the other two (#2 and #4) were yellow phase. The single layer of  $\text{Al}_2\text{O}_3$  coating (ELAN Ltd.) was centered at 1280 nm for the signal wavelength but reduced substantially the Fresnel losses also at the pump wavelength of 1064 nm. The aperture of the plates was roughly  $10 \times 10 \text{ mm}^2$ , the thickness varied from 2.14 to 2.44 mm and the wedge was between  $10''$  and  $30''$ . The cut angle was  $\theta \sim 45^\circ$  while  $\phi = 0^\circ$  (plate #1) and  $\phi = 45^\circ$  (plates #2-4). We simultaneously tested a yellow color sample of  $\text{CdGa}_2\text{S}_4$  (CGS) with a diameter of 12.5 mm and thickness of 1.6 mm which was cut at  $\phi = 45^\circ$  and  $\theta = 45^\circ$ . However, this disk had a different AR-coating, on both sides, performed by QTF Inc. using multilayer structure specified for  $< 1\%$  reflection at 1064, 1274 and 6450 nm. Such CGS samples had been tested before with a similar laser source as the one described below but with pulse duration of 14 ns and no damage was observed up to peak on-axis fluence of  $1.6 \text{ J/cm}^2$  using unfocused beam with a diameter of  $\sim 3.8 \text{ mm}$ .

The HGS samples are normally single pass saw cut in the crystallographic frame and then polished using alumina particles involving several polishing stages with decreasing grit sizes of 40, 20, 7, 1 and  $0.5 \mu\text{m}$ .

The irradiating source was the same as used for OPO pumping: a diode-pumped Q-switched Nd:YAG laser/amplifier at 1064 nm with a pulse duration of 8 ns operating at 100 Hz. Intensity spatial profile is close to Gaussian distribution and  $M^2 \sim 1.4$ . The linearly polarized beam passed through plates # 1, 2 and 4 as e-wave and through plate # 3 as o-wave, its orientation relative to the CGS sample was unknown. The beam was focused with a lens with a focal length of 250 mm and the samples to be tested were placed slightly behind the focus where the area amounted to  $S = \pi w^2 = 1.13 \times 10^{-3} \text{ cm}^2$ , with  $w$  denoting the  $e^{-2}$  intensity radius. The pulse energy  $E$  was varied by a system of a half-wave plate and a polarizer and measured directly in front of the sample with pyroelectric detector. All fluence values given below are peak-on-axis, i.e.  $\sim 2 * E/S$ .

Damage threshold of every plate was determined according to the modified procedure S-on-1, recommended by ISO [32]. Using the S-on-1 method which defines a 0% probability for damage as a more rigorous definition of laser damage threshold than the method of simply increasing the incident fluence until damage occurs gives significantly lower values as observed in  $\text{ZnGeP}_2$  at its OPO pump wavelength [33]. The small spot provided the opportunity to effectively use the test plate surfaces. 14 sites on every plate, or 7 on each side, were randomly chosen for irradiation. Every site on a given plate was irradiated in a series of exposures, starting from an energy level similar for all sites on a given plate until damage occurred. Thus, damage probability at a given energy level could be calculated as a ratio of number of sites damaged at energies lower or equal to this level to full number of tested sites 14. The obtained distribution of damage probabilities versus energy fluence was then fitted with a linear function which gave the 0% damage probability for a given plate as the intercept with the energy fluence coordinate axis. Two or three sites on each plate were irradiated before starting the test to estimate expected damage threshold. The exposure time in the tests was 1 min (6000 pulses) and the step between two subsequent exposures was  $0.07 \text{ J/cm}^2$  in terms of peak-on-axis energy fluence.

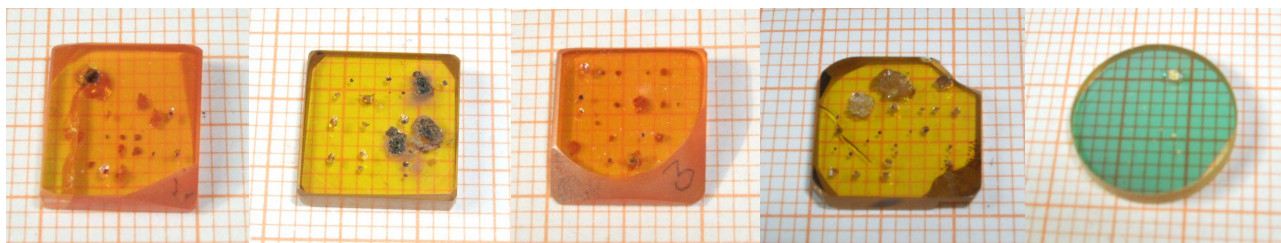


Fig. 3. HGS damage test plates #1 to #4 and CGS damage test disk. The small spots are from the damage test described in this section while the larger damages are result of other experiments with larger beam area, see Section 5.

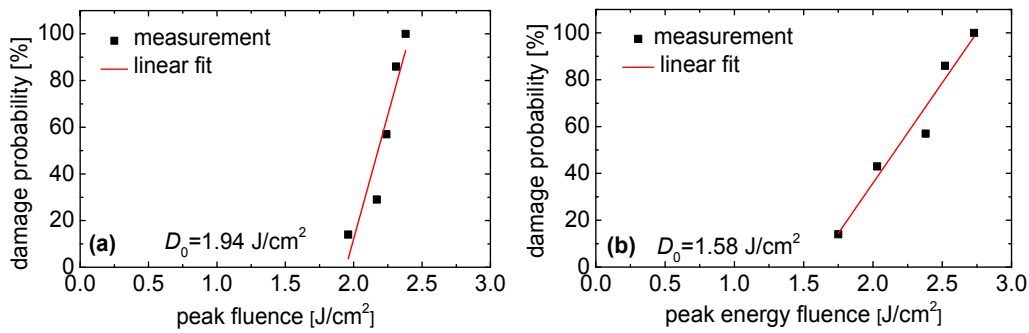


Fig. 4. Damage probability for the single side AR-coated HGS test plate #1 when the front surface is the AR-coated one (a) and when the front surface is the uncoated one (b).  $D_0$ : 0-probability damage threshold.

Figure 4 shows the results obtained with HGS test plate #1 when 7 sites were illuminated in each direction. When the AR-coated surface was front surface a total of 5 damages appeared on the rear (uncoated) side and 4 damages on the front AR-coated side. When the uncoated surface was front surface a total of 2 damages appeared on the front uncoated side and 5 damages on the rear AR-coated side. Thus, it cannot be concluded that AR-coating improves the damage resistivity as observed in  $\text{ZnGeP}_2$  [33] because in total 7 damage spots on the uncoated against 9 damage spots on the AR-coated side occurred. Although the linear fits in Fig. 4 have different slopes for the two propagation directions the results can be combined into one plot (Fig. 5a) whose linear fit gives a 0-probability damage threshold of  $1.76 \text{ J/cm}^2$ . HGS test plates #2 and #4 showed lower damage resistivity in both directions compared to #1 and all damages appeared on the AR-coated side. HGS test plate #3 had an overall damage threshold higher than #1 but also here all damage craters occurred on the AR-coated side. In the double side AR-coated CGS disk most damages occurred on the rear side. The damage threshold was higher (Fig. 5b) and the increased slope indicates a more even distribution of surface defects compared with HGS.

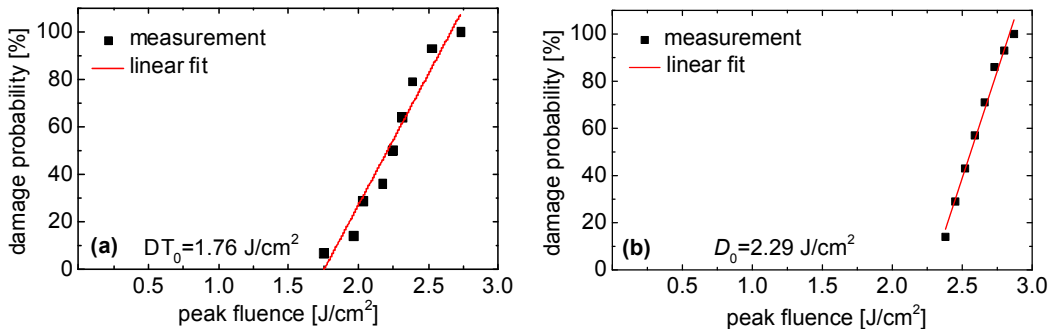


Fig. 5. Average damage probability from illumination in both directions for the single side AR-coated HGS test plate #1 (a) and double side AR-coated CGS test disk (b).  $D_0$ : 0-probability damage threshold.

Table 3. Summary of 0-probability damage threshold determination in HGS and CGS test plates in terms of peak on-axis fluence.

Damage test sample	AR-coated front surface $D_0$ [ $\text{J/cm}^2$ ]	Uncoated front surface $D_0$ [ $\text{J/cm}^2$ ]	Overall $D_0$ [ $\text{J/cm}^2$ ]
HGS plate #1,	1.94	1.58	1.76
HGS plate #2	1.73	1.18	1.37
HGS plate #3	1.88	1.98	1.58
HGS plate #4	0.96	1.44	1.68
CGS disk	2.29	-	2.29

It should be outlined, however, that in some cases the fits were not good due to the small number of tested sites if compared to [33]. This is especially true for the lowest values in the second and third column of Table 3 which

summarizes the results. Thus for the fit giving  $0.96 \text{ J/cm}^2$  in fact no damage was observed below  $2.3 \text{ J/cm}^2$  while for the fit giving  $1.18 \text{ J/cm}^2$  no damage occurred below  $1.5 \text{ J/cm}^2$ . Obviously these 2 cases should be excluded when making conclusions as can be seen from the values of the overall fit in the last table column. Taking an average of these values the 0-probability damage threshold for HGS is  $(1.6 \pm 0.2) \text{ J/cm}^2$  which translates into  $200 \text{ MW/cm}^2$  and is rather high.

For the above reason we calculated from the experimental data also average damage thresholds  $D_m = \frac{\sum D_i n_i}{N}$ , and average error of the mean  $s$  from  $s^2 = \frac{\sum (D_m - D_i)^2 n_i}{N(N-1)}$ , where  $N$  is total number of damaged sites,  $N = n_1 + n_2 + \dots$ ,  $N=7$  or  $14$  in our case. One can define the probability  $P$  for the damage threshold  $D$  to be e.g. in the interval  $D_m \pm 3s$ , then  $P(N=7)=98\%$  and  $P(N=14)=99\%$ . But one can also fix the probability and leave  $k$  as a variable in  $D_m \pm ks$ . Table 4 shows the results of such a processing of the damage threshold data.

Table 4. Summary of the average damage threshold values in terms of peak on-axis fluence and the deviation for 94% probability.

Damage test sample	AR-coated front surface		Uncoated front surface.	
	Damage of front surface, [J/cm <sup>2</sup> ]	Damage of rear surface, [J/cm <sup>2</sup> ]	Damage of front surface, [J/cm <sup>2</sup> ]	Damage of rear surface, [J/cm <sup>2</sup> ]
HGS plate #1	$D_m=2.29, s=0.03$ $D=(2.29 \pm 0.09)$	$D_m=2.28, s=0.05$ $D=(2.28 \pm 0.15)$	$D_m=2.52$	$D_m=2.05, s=0.13$ $D=(2.05 \pm 0.39)$
HGS plate #2	$D_m=2.38, s=0.08$ $D=(2.38 \pm 0.21)$	$D_m \geq 2.59$	$D_m \geq 2.45$	$D_m=1.89, s=0.14$ $D=(1.89 \pm 0.32)$
HGS plate #3	$D_m=2.76, s=0.10$ $D=(2.76 \pm 0.26)$	$D_m \geq 3.01$	$D_m \geq 2.45$	$D_m=2.26, s=0.04$ $D=(2.26 \pm 0.10)$
HGS plate #4	$D_m=2.33, s=0.02$ $D=(2.33 \pm 0.05)$	$D_m \geq 2.45$	$D_m \geq 2.45$	$D_m=2.11, s=0.08$ $D=(2.11 \pm 0.19)$
CGS disk	-	$D_m=2.60, s=0.04$ $D=(2.60 \pm 0.09)$	-	-

The results in Table 4 can be used to obtain an average value for uncoated HGS. Combining the values when this surface was damaged as front and as rear surface one obtains  $D=(2.52 \pm 0.18) \text{ J/cm}^2$ , for 94% probability. The damage threshold of AR-coated surface of HGS when this surface is front surface can be obtained by combining the results of the corresponding column in Table 4 as four independent measurements, each of them with equal weight and its own error which gives  $D=(2.44 \pm 0.10) \text{ J/cm}^2$ , for 94% probability. Similarly, the damage threshold of AR-coated surface when it is rear surface amounts to  $D=(2.08 \pm 0.16) \text{ J/cm}^2$ , for 94% probability.

A different approach is also possible for the results concerning the AR-coated surface of HGS considering all the data on different samples as independent measurements. This (apparently more physical) approach leads to  $D=(2.44 \pm 0.11) \text{ J/cm}^2$  and  $D=(2.07 \pm 0.13) \text{ J/cm}^2$ , when the AR-side is front and rear surface, respectively, for 94% probability in both cases. Obviously the two approaches yield almost the same results for the damage threshold of the AR coated HGS.

Concluding, damage threshold of HGS under these conditions is very high and seems not to depend on color (phase). AR-coating does not improve it so far but also does not seriously reduce the surface damage threshold of the front surface. There is definitely dependence on the band-gap, however, because CGS showed higher damage threshold even with multi-layer AR coating. We have no real explanation why the damage resistivity of AR-coated HGS is lower when this surface is rear surface in experiments with slightly diverging beam. In fact opposite trend has been described for  $\text{ZnGeP}_2$  [33,34], but in this case, as already mentioned, the AR-coating improved the  $\text{ZnGeP}_2$  surface damage resistivity. The “anomaly” in our case could be associated with some bulk effect because the trend seems more general if we take into account the results with the uncoated surface damage tests of HGS and also the double side AR-coated CGS.

## 5. OPTICAL DAMAGE OF HGS WITH UNFOCUSED BEAMS INSIDE AND OUTSIDE THE OPO

Optical damage in HGS occurred at much lower fluence values when such active elements were used in OPOs with large beam sizes (diameters). For the OPO element HGS-1 cut for 4- $\mu\text{m}$  generation, see Fig. 1, bulk damage was observed at about  $0.3 \text{ J/cm}^2$  ( $37.5 \text{ MW/cm}^2$ ) of peak pump fluence (intensity) after hours of operation when the signal wave was present in the OPO which corresponds to  $\sim 95 \text{ mJ}$  in Fig. 2b, i.e. very close to the maximum pump level applied at 100 Hz. These are incident values and one should bear in mind that there is a double pump pass in this OPO. The damage was a white scattering cloud – one of the rare observations of bulk damage instead of surface damage, see Fig. 6.

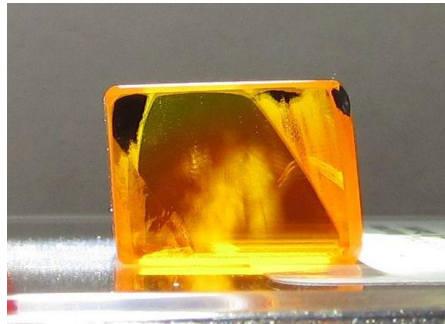


Fig. 6. Bulk damage occurring in the type-I orange phase HGS-1 OPO element generating 4  $\mu\text{m}$  idler pulses after using it for hours at  $\sim 95 \text{ mJ}$  pump energy and 100 Hz.

While such bulk damage could be hardly observable in the thin plates considered in the previous section, this HGS-1 OPO element was with unknown AR-coating, hence, we focused our attention further on HGS-2 which had the same AR-coating type as the thin damage test plates of HGS described in Section 4. We observed formation of similar white clouds inside this type-II HGS crystal when deployed in the double pump pass OPO for idler generation at 6.3  $\mu\text{m}$ . Above 100 mJ of pump energy they formed quickly (within 30 min) at 100 Hz and this was the main reason to characterize this OPO at 10 Hz. Figure 7 illustrates the formation of such bulk damage in the HGS-2 OPO element under  $>100 \text{ mJ}$  of pump energy ( $>0.32 \text{ J/cm}^2$  peak fluence) at 10 Hz. Note that in order to see the cloud, it is necessary to illuminate the crystal with white light. The bulk damage leads to significant reduction of the crystal transmission: with a small (less than the damage size) continuous-wave (cw) probe beam at 1064 nm we measured about 10% decrease of the transmission for o-polarization and up to 40% for the e-polarization. With larger beams the transmission reduction was smeared to  $<5\%$ . It should be mentioned here, that no bulk damage occurred in HGS when the active element was rotated in the cavity by  $90^\circ$  so that no oscillation was possible.

At maximum pump energy of 140 mJ (on-axis fluence of  $0.44 \text{ J/cm}^2$ ), see Fig. 2c, eventually first signs of surface damage were seen, though operating at 10 Hz, in the form of dark (burned) spot on the AR-coating, normally on the side towards the closer cavity mirror. For this pump level we observed intracavity surface damage also when the OPO was not perfectly aligned, generating an idler energy of 1.7 mJ at 10 Hz, compare Fig. 2c. This is illustrated in Fig. 8. Note that bulk damage in the form of scattering cloud had already occurred beneath the surface spot in the same position. It should be noted that at the maximum pump fluence we observed few times also damage to the Ag total reflector, Fig. 1.



Fig. 7. Bulk damage occurring in the type-II orange phase HGS-2 OPO element generating 6.3  $\mu\text{m}$  idler pulses after using it for hours at  $>100 \text{ mJ}$  pump energy and 10 Hz.

To verify that this kind of damage is partially related to the signal wave we immediately proved that no damage occurred to a thick (9.4 mm) sample of yellow phase HGS (see Fig. 9 left) irradiating it with 100 mJ of pump energy at 100 Hz outside the cavity. In this case the beam diameter was reduced to 5 mm (cross section of  $0.2 \text{ cm}^2$ ) which corresponds to  $>1 \text{ J/cm}^2$  peak axial fluence in single pass but no signs of any damage including bulk clouds were seen after illumination for 15 min. Since this sample was uncoated the conclusion basically concerns bulk damage. It is, however, difficult to separate the contribution of signal and pump to the crystal damage occurring when the OPO is operating since the oscillating signal depletes the central part of the pump.



Fig. 8. Surface damage on the HGS-2 OPO element generating  $6.3 \mu\text{m}$  idler pulses at 140 mJ pump energy and 10 Hz.

In view of the bulk damage observed in the OPO prior to surface damage, we decided to test available thick samples outside the OPO cavity. These samples shown in Fig. 9 illustrate also the different phases of this nonlinear material.

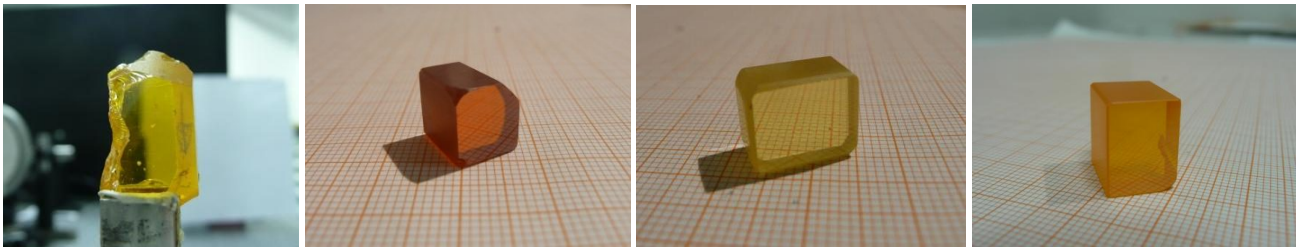


Fig. 9. Thick damage test elements HGS-Y, HGS-O, CGS, and CHGS (from left to right) as described in the text.

From left to right on Fig. 9 these were: a 9.4-mm thick yellow phase HGS (HGS-Y) with unknown orientation and very poor surface polish, an orange colour HGS sample HGS-O cut at  $\varphi=0^\circ$ ,  $\theta=56^\circ$ , i.e. for type-II phase-matching, with an aperture of  $9.23 \times 10 \text{ mm}^2$ , length of 10.75 mm, and wedge of  $\sim 4\text{-}5^\circ$ , whose surface quality was also poor, a light yellow colour CGS, with an aperture of  $12.6 \times 10.5 \text{ mm}^2$ , length of 7 mm and unknown orientation, and a dark yellow  $\text{Cd}_{0.27}\text{Hg}_{0.73}\text{Ga}_2\text{S}_4$  (composition in the charge) sample CHGS with an aperture of  $13.38 \times 10.08 \text{ mm}^2$  and thickness of 13.62 mm with orientation  $\varphi=45^\circ$ ,  $\theta=60^\circ$ .

First of all we performed some cw damage tests to rule out effects from the average power like macroscopic heating. The cw laser at 1064 nm had an elliptic beam cross section with Gaussian diameters of 1.78 and 1.57 mm in the horizontal and vertical planes, respectively, or an area of  $0.022 \text{ cm}^2$  in the position of the crystal tested. Crystals HGS-Y and HGS-O were tested for exposition of 7 min and no damage of any kind occurred up to 5.5 W of incident power which corresponds to a peak on-axis cw intensity of  $>500 \text{ W/cm}^2$ . This is more than an order of magnitude higher than the maximum values in the 100 Hz HGS OPO (Fig. 2b) having in mind that the beam cross section is 29 times smaller in the cw case while the maximum average power applied in the OPO was 10 W. It is also 5 times higher than in the extracavity damage test of HGS-Y (100 mJ, 8 ns pulses at 100 Hz) described just above which also produced no damage.

Then we proceeded with damage tests using the 8 ns 1064 nm pump laser at 100 Hz choosing a cross section of  $0.11 \text{ cm}^2$  or diameters of 3.65 and 3.86 mm in the horizontal and vertical direction, respectively, sufficient to cause damage with the available pump energy of 150 mJ. The tests were for 10 min with interruption of 2 min between the measurements, starting from 30 mJ and increasing the energy by 10 mJ in each step.

Table 5. Summary of the average damage threshold values in terms of peak on-axis fluence and the deviation for 94% probability.

Damage test sample	Average damage threshold, [J/cm <sup>2</sup> ]	Damage on surface
HGS-Y	$D=(1.50 \pm 0.28)$	rear (2), front (1), both (1)
HGS-O	$D=(1.09 \pm 0.22)$	rear (3), front (1)
CGS	$D=(2.18 \pm 0.22)$	rear (4)
CHGS	$D=(1.23 \pm 0.26)$	rear (4)

Four tests were performed with each of the uncoated samples and the results are summarized in Table 5. Figure 10 shows crystal shadow patterns obtained by scattered He-Ne laser light illustrating the damages.

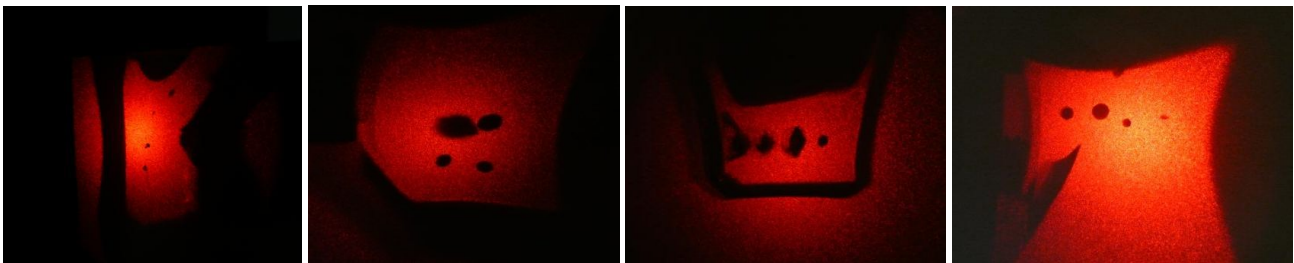


Fig. 10. Crystal shadow patterns for HGS-Y, HGS-O, CGS, and CHGS (from left to right) each with 4 damage spots.

The damage thresholds determined here are systematically lower than the results described in the previous section with focused beams. The main difference is the beam cross section which was roughly 100 times smaller in Section 4. In particular, comparing uncoated HGS, its damage threshold is about 2 times higher for small beam sizes. For CGS, however, this is not necessarily true. One can compare the present results also with the estimation of 2.4 J/cm<sup>2</sup> (peak on-axis) for orange phase HGS from single shot tests with a beam diameter of 0.4 mm (focused beam with a spot area of 0.0013 cm<sup>2</sup>) using 30 ns pulses at 1064 nm [35] and this supports the above conclusion.



Fig. 11. Rear surface crack observed in CGS.

Surface damage occurs mostly on the rear surface, front surface damages are exceptions and no changes in the bulk were observed such as white clouds. However, just before the breakdown, white light is seen in the bulk. Sometimes such flash of light is seen also at energies close to the damage limit. In CGS, when the rear surface is damaged it is not simply a black spot from the breakdown but also a crack (see Fig. 11).

Since no bulk damage was observed in these experiments we conducted also few longer (60 min) tests at fluence levels below the corresponding surface damage threshold and all other conditions unchanged. At 41.5 mJ incident energy corresponding to peak on-axis fluence of  $0.755 \text{ J/cm}^2$  no signs of damage were seen in HGS-O and the HGS-2 AR-coated OPO element from Figs. 1,7,8. In CHGS no damage was seen at 50 mJ or  $0.91 \text{ J/cm}^2$  while in CGS no damage occurred at 82.5mJ or  $1.5 \text{ J/cm}^2$ . The only bulk damage observation in the form of clouds was with HGS-O at 45 mJ or  $0.82 \text{ J/cm}^2$ . This single observation is still evidence that bulk damage can occur solely due to the 1064 nm pump light.

Since the OPOs are pumped in double pass, we tested some of the thick samples also in double pass using an Ag retroreflector for 10 min long exposition tests: surface damage occurred at lower incident fluence, at  $0.73 \text{ J/cm}^2$  (40 mJ) in HGS-O (front side) and at  $0.76 \text{ J/cm}^2$  (42 mJ) for CHGS (rear side) but no bulk damage was observed. Decreasing the incident fluence to  $0.45 \text{ J/cm}^2$  (25 mJ) in longer (60 min) tests no bulk damage in the form of clouds occurred in HGS-O and the AR-coated orange phase HGS-2 OPO element. The latter is a clear indication that bulk damage has lower threshold in the presence of the signal wave when the HGS crystal is inside the operating OPO. Concerning surface damage, the threshold values (fluence) are about 50% higher than inside the OPO. Having in mind that surface damage occurs apparently independent of the repetition rate and the fact that we compare uncoated orange HGS in the extracavity test with AR-coated HGS in the OPO the difference seems not so dramatic, i.e. the increase of the surface damage probability inside the OPO cavity is much less pronounced than the susceptibility to bulk damage formation.

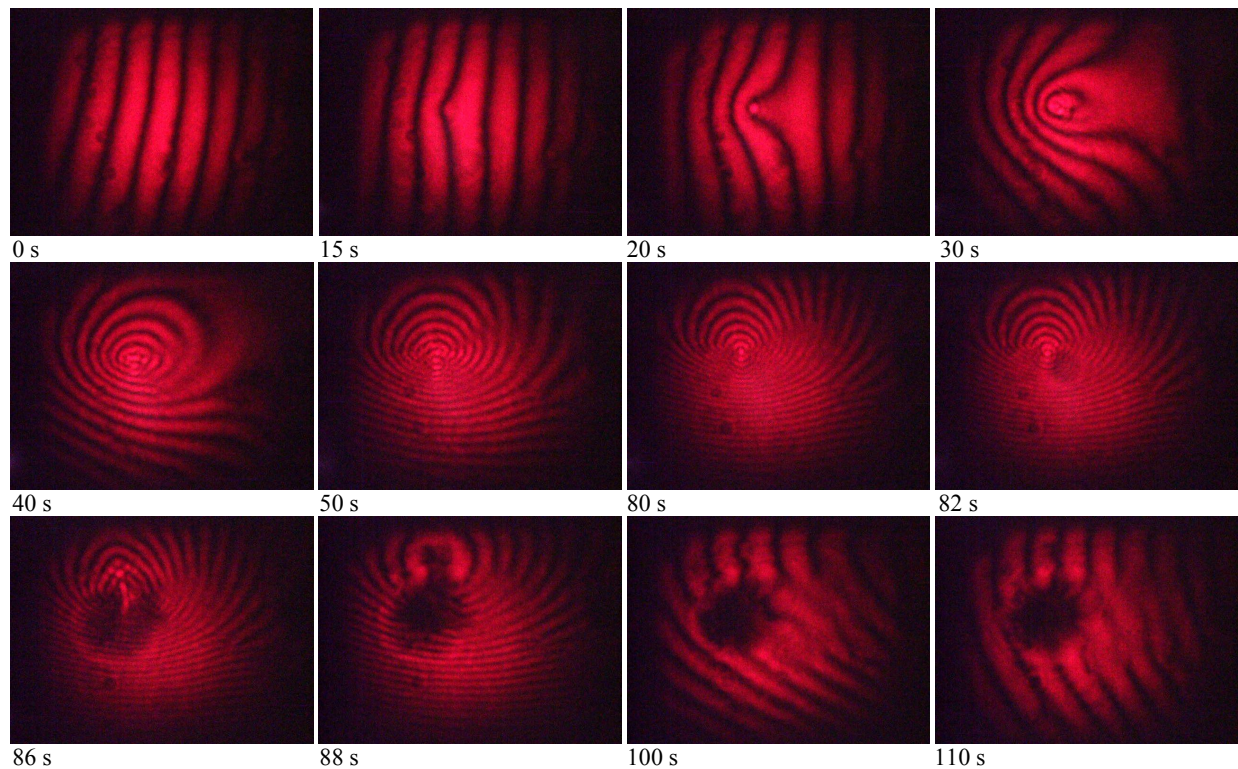


Fig. 12. Damage of the front AR-coated surface of orange HGS recorded at  $0.8 \text{ J/cm}^2$  fluence at 1064 nm and 100 Hz: Irradiation starts from the 10<sup>th</sup> second and heating centered in the beam is modifying the interference pattern, small damage occurs at 82 s, however, off the center, and full damage at 88 s, at 90 s the irradiation is stopped and the interference fringes start moving backwards.

Finally, in Fig. 12 we illustrate the process of surface damage formation at large (unfocused) beam sizes in HGS. The sample is the orange phase HGS plate #3 shown in Fig. 3 where such damages can be seen as large spots. Figure 12 consist of snapshots from a video recorded at incident energy of  $\sim 45 \text{ mJ}$  at 100 Hz. For a pump spot of  $3.65 \times 3.86 \text{ mm}^2$  (diameters), this corresponds roughly to  $0.8 \text{ J/cm}^2$  which is above the damage threshold of the AR-coated front surface.

## 6. OPTICAL DAMAGE OF BGS AND BGSe

Damage tests of uncoated BGS and BGSe samples were performed with 14-ns and 1-ns long pulses at 1064 nm at repetition rates of 100 and 500 Hz, respectively. The test plates had an aperture of  $8 \times 8 \text{ mm}^2$  and thickness of 2.2 mm for BGS and BGSe-z (z-cut plate) and 2.3 mm for BGS-y (y-cut plate), see Fig. 13.



Fig. 13. Damage test plates BGS, BGSe-y, BGSe-z, and damage on test plate BGS (from left to right).

The same OPO pump source at 1064 nm as described before but with 14-ns pulse duration was used in the first series of experiments at 100 Hz. The laser beam of 3.8 mm diameter was used without further focusing for BGSe-y (spot area of  $\sim 0.11 \text{ cm}^2$ ) and additionally focused with a 25-cm lens for the BGS and BGSe-z test plates which were placed behind the focus where beam diameters were 1.7 mm (horizontal) and 2.24 mm (vertical) corresponding to a spot size of  $\sim 0.03 \text{ cm}^2$  at  $e^{-2}$  intensity level. The energy incident on the plate was varied by a system of half-wave plate and Glan polarizer.

The BGS test plate was exposed to laser radiation for a period of 1 min (6000 pulses) and the time interval between two successive exposures was 2 min. The measurement started at a level of  $0.6 \text{ J/cm}^2$  (incident peak-on-axis energy fluence) increasing it with a step of  $0.2 \text{ J/cm}^2$ . The damage threshold was determined as the arithmetic average between the last measurement without any visible changes in this test plate (at  $3.6 \text{ J/cm}^2$ ) and the energy at which first signs of damage were observable ( $3.8 \text{ J/cm}^2$ ), i.e. we obtained  $3.7 \text{ J/cm}^2$  of incident peak-on-axis energy fluence (or  $264 \text{ MW/cm}^2$  of peak-on-axis intensity) as a characteristic damage threshold. This is an exceptionally high value for a non-oxide nonlinear crystal transparent in the mid-IR and compares only with measurements in LGS crystals, see Section 2. The damage observed was a small crater on the rear surface of the plate that appeared after an exposition time of 5 s.

The BGSe-z test plate was tested in a similar manner starting at a level of  $0.6 \text{ J/cm}^2$  and increasing it with a step of  $0.1 \text{ J/cm}^2$ . The last measurement without any visible changes in this test plate was at  $1.4 \text{ J/cm}^2$  while at  $1.5 \text{ J/cm}^2$  a small crater appeared on the rear surface of the plate after an exposition time of 5 s. Thus the surface damage threshold amounts to  $1.45 \text{ J/cm}^2$  of incident peak on-axis energy fluence (or  $104 \text{ MW/cm}^2$  of peak on-axis intensity).

The BGSe-y test plate was tested in the same manner as BGSe-z but with the unfocused beam. The last measurement without any visible changes in the test plate was at  $1.2 \text{ J/cm}^2$  while at  $1.3 \text{ J/cm}^2$  three small spots (craters) appeared on the rear surface which had worse quality after an exposure time of 25 s. Thus the surface damage threshold amounts to  $1.25 \text{ J/cm}^2$  of incident peak on-axis energy fluence (or  $89 \text{ MW/cm}^2$  of peak on-axis intensity).

Table 6. Summary of damage threshold values measured at 1064 nm for BGS and BGSe at different pulse durations.

Damage test sample	14 ns, 100 Hz			1 ns, 500 Hz		
	beam area [ $\text{cm}^2$ ]	damage threshold [ $\text{J/cm}^2$ ]	damaged description	beam area [ $\text{cm}^2$ ]	damage threshold [ $\text{J/cm}^2$ ]	damaged surface description
BGS	$\sim 0.03$	3.7	crater on rear surface after 500 shots	0.00031	2.9	crater on rear surface after 6000 shots
BGSe-y	$\sim 0.11$	1.25	crater on rear surface after 2500 shots	0.00146	0.55	whiter spot / bulk darkening after 6000 shots
BGSe-z	$\sim 0.03$	1.45	crater on rear surface after 500 shots	0.00152	1.02	small crater on rear surface after 1500 shots

There is a recent measurement of surface damage for BGSe also by other authors with which one can compare:  $2.8 \text{ J/cm}^2$  for 5 ns pulses at 1 Hz [36]. This value is measured with a beam diameter of 0.4 mm on a 2-mm thick plate using the 1-

on-1 procedure for 20% damage probability [32]. That it is higher than in Table 6 can be attributed to the smaller beam size used as we observed for HGS.

The beam from the regenerative amplifier delivering 1 ns, 1064 nm pulses at 500 Hz repetition rate had a diameter of 3 mm and was also focused with a 25-cm lens. Similar tests were performed as described above, the exposure time was 12 sec and the time interval between two exposures was 1 min. The BGS test plate was tested behind the focus where the beam diameter of 0.2 mm corresponded to a cross section of  $0.31 \times 10^{-3} \text{ cm}^2$  at intensity level of  $e^{-2}$ , starting from  $1.2 \text{ J/cm}^2$  of incident peak-on-axis energy fluence with a step of  $0.2 \text{ J/cm}^2$ . The damage threshold obtained in the same manner between two steps amounted to  $2.9 \text{ J/cm}^2$  of incident peak-on-axis energy fluence. The damage observed was again a crater on the rear surface of the plate. This damage threshold in terms of fluence is lower than with 14 ns pulses although the beam cross section is much smaller. However, in terms of peak on-axis intensity it corresponds to  $2.9 \text{ GW/cm}^2$  which emphasized the combined fluence/intensity dependence of the damage threshold for such pulse durations as mentioned in the Introduction.

The BGSe-y plate was positioned at a beam diameter of 0.43 mm corresponding to a cross section of  $1.46 \times 10^{-3} \text{ cm}^2$  at intensity level of  $e^{-2}$ , the damage tests started from  $0.2 \text{ J/cm}^2$  of incident peak on-axis energy fluence with a step of  $0.05 \text{ J/cm}^2$ . Dark spot appeared at  $0.6 \text{ J/cm}^2$  and before it, from about  $0.5 \text{ J/cm}^2$ , some decoloration of the illuminated spot was observed. The BGSe-z plate was positioned at a beam diameter of 0.44 mm corresponding to a cross section of  $1.52 \times 10^{-3} \text{ cm}^2$  at intensity level of  $e^{-2}$ , the damage tests started from  $0.2 \text{ J/cm}^2$  of incident peak on-axis energy fluence with a step of  $0.05 \text{ J/cm}^2$ . A small crater appeared on the rear surface at  $1.05 \text{ J/cm}^2$ . Also in this sample some decoloration was observed at lower intensities ( $\sim 0.7 \text{ J/cm}^2$ ). This effect looks like increased transmission in the visible, it was difficult so see how deep it extends from the surface and sometimes it turned out to be reversible. Thus the surface damage threshold measured with BGSe-z should be representative of this compound and the value in Table 6 is substantially lower than for the sulfide BGS. Moreover, the selenide BGSe shows also some susceptibility to bulk damage formation at lower fluence although these were not scattering centers as observed in HGS.

No crystal damage problems occurred in the BGS OPO presented in Fig. 2a, with maximum pump levels limited by damage to the metallic total reflector, similar to the observations we made with the HGS-2 OPO element.

## 7. CONCLUSION

While HGS is probably the best nonlinear crystal for 1- $\mu\text{m}$  pumped mid-IR down-conversion its performance in nanosecond OPOs is severely limited by optical damage. Surface damage in extracavity experiments depends on the beam size and occurs at lower fluence at 1064 nm for larger beam sizes which is related to the probability to find a surface defect within the illuminated spot. AR-coatings at present seem not to improve the surface damage resistivity of HGS and there is obviously a room for improvement. However, at present this turns out to be a secondary problem because bulk damage in the form of scattering centers (white clouds) occurs at lower pump levels at 1064 nm. We cannot rule out that surface damage is a consequence of bulk and under-surface damage in the cases when such occur. The observation of lower bulk damage thresholds contradicts the widely spread opinion that surface damage of such nonlinear crystals is the main limitation. Bulk damage can be observed when illuminating the crystal only by pump pulses at 1064 nm, however, such damage occurs at substantially lower levels when the crystal is deployed in the OPO and the circulating signal power is sufficiently high. The minimum pump fluence for which we observed strong formation of such defects in a double pass pumped HGS OPO at 100 Hz was  $0.3 \text{ J/cm}^2$  but the threshold should be even lower because the detection limit depends on the illumination time. Thus, reduction of the repetition rate does not solve the problem and there is no "cumulative" damage, only the process of defect formation is slowed down. Surface damage in the OPO occurs also at lower pump levels than extracavity but this is still at least 50% above the bulk damage threshold of orange phase HGS. Nevertheless, comparison of single pass and double pass damage tests with intracavity surface damage observations, in particular when the OPO is misaligned, indicates reasonable correspondence and hence no essential contribution of the other two waves (signal or idler) to the surface damage formation.

The existence of different phases (stoichiometry) of HGS additionally complicates the study of light induced optical damage. As could be expected, yellow phase HGS or Cd doped HGS exhibit higher surface damage threshold but this seems systematically confirmed only for large beam sizes, with focused beams, when the surface damage threshold is above  $2 \text{ J/cm}^2$  no significant difference between the phases is evident. We never observed bulk damage in the form of clouds in yellow phase HGS but unfortunately no AR-coated samples of this phase were available for intracavity OPO

tests. CGS exhibited the highest damage resistivity and this seems also related to lowest concentration of defects. The surface damage resistivity of CGS seems not deteriorated by AR-coating and can serve as an orientation for the maximum achievable damage resistivity of HGS which should be  $>2 \text{ J/cm}^2$  in terms of peak on-axis fluence.

We associate the lower damage resistivity of HGS when used in the OPO with the signal wave because it is resonated and is much closer to the band-gap but there is no direct evidence that it is the signal and not the idler wave (Note that resonating the idler as suggested in early OPO literature is not a solution because such dielectric mirrors have themselves low damage resistivity). In any case the damage effect is not related to a resonance because we observed bulk damage formation at different signal wavelengths (OPOs generating 4.03 and 6.3  $\mu\text{m}$  idler output, Fig. 2). In fact, for the OPO elements studied here the residual absorption at the signal wave was very low, typically  $<2\%/cm$ , while the idler absorption at 6.3  $\mu\text{m}$  was typically 10%/cm or even more. We have no explanation for the large residual mid-IR absorption of the present HGS samples and this will be studied in the near future. In any case comparative transmission measurements of thick samples in the mid-IR indicate that orange phase HGS exhibits reduced transmission compared to yellow phase HGS or CGS. Moreover, the transmission of orange HGS decreases significantly starting from  $\sim 4 \mu\text{m}$  while that of yellow HGS and CGS does not change up to  $\sim 9 \mu\text{m}$ . We performed some preliminary extracavity damage tests using the idler OPO output at 6.3  $\mu\text{m}$  and 10 Hz repetition rate but the achievable focused fluence was limited. In any case no visible damage was detected in the HGS-O test element up to a peak fluence of  $0.6 \text{ J/cm}^2$  in the focal spot of 0.22 mm diameter (area of  $4 \times 10^{-4} \text{ cm}^2$ ) in two runs of 10 min each, which is an evidence that at least idler alone is not the main damage factor inside the OPO.

In support of the role of the signal wave, it should be outlined that the signal pulses in such OPOs make many round trips and experience multiple absorption losses. Thus a great part of their energy is absorbed in the nonlinear crystal. Increasing the output coupling has been often considered in the literature as a solution to reduce the intracavity signal power but for the present singly resonant OPOs the oscillation threshold is already too high to afford increased signal losses. In the extreme limit of no output coupler highly nonlinear crystals as HGS could operate as optical parametric generators or OPOs with low finesse due to idler reflectivity of the crystal faces [37]. Indeed, removing the output coupler from the set-up in Fig. 1, with the HGS-2 crystal for 6.3  $\mu\text{m}$  generation, we observed such operation with slightly higher threshold but lower slope efficiency which resulted in maximum conversion efficiency of 1.4% from pump to idler (compare with Fig. 2c) or 2.06 mJ of idler energy at 147 mJ incident pump energy. No bulk damage was observed in this experiment which means that conversion efficiency could be possibly improved by using tighter focusing in comparison to the OPO case. Note that this set-up is also equivalent to the use of HGS as optical parametric amplifier (OPA) because the scheme is double pass and the beam cross section can be varied in the two passes.

From practical point of view the information extracted from extracavity measurements seems of limited value because it is difficult to simulate the situation in the OPO in the presence of more waves. Testing of passive (non-phase-matched) elements in the OPO cavity is not expected to provide more information than inspecting the OPO element itself. Thus, our primary interest in the future will be manufacturing of yellow phase HGS active elements and their test in the OPO. This is absolutely important for the HGS crystal because the present situation indicates very low damage resistivity (comparable to many other chalcogenide mid-IR crystals applicable for 1- $\mu\text{m}$  pumping) and similar to CSP, energy scaling is limited notwithstanding the high figure of merit of HGS.

The successful OPO operation of BGS is evidence that the nonlinear figure of merit cannot be the only criterion for selection of the best NLC. Even if the FM is so low that it is comparable with the best oxide NLCs, non-oxide NLCs transparent in the mid-IR that exhibit exceptionally high damage resistivity are potentially very interesting simply because their use seems more reliable and the approach to improve their performance in the future is more straightforward – growth of larger size crystals. We have identified so far two such NLCs, BGS and LGS, and their high damage resistivity seems related to their large band-gaps – both compounds are colorless when free of defects in stoichiometric composition. The damage tests themselves were more reproducible in these crystals, bulk damage was never observed, and the results were rather insensitive to the surface quality or the presence or not of AR-coating. Since CGS is another such NLC (unfortunately lacking sufficient birefringence) that can also be grown colorless, we conclude that these properties are possibly related to lower concentration of defects leading also to weaker dependence of the damage threshold on the beam size.

It is difficult to predict if it will be possible in the future to grow larger sizes of BGS or LGS crystals and even more difficult if it will be possible to understand the defect formation mechanisms in HGS and find an appropriate solution. In any case, when OPO operation is limited by crystal damage, one has to search for alternative strategies how to avoid it. Some of them are known, e.g. using top-hat pump beam profiles to avoid the on-axis peak of the intensity. Other

approaches for homogenization of the spatial beam profile and phase like the RISTRA concept have proven very effective in mid-IR OPOs pumped in the 2- $\mu\text{m}$  range [38]. The fluence dependence of the damage threshold also indicates that using shorter pump pulses (e.g. 1 ns) is another alternative [24]. Pulses of  $\sim 1$  ns duration could be advantageous also for adding an OPA stage with sufficient gain, i.e. relaxing the energy requirements to the OPO and boosting the output in a subsequent OPA stage, but this will require the development of novel, non-standard laser pump systems [39].

## ACKNOWLEDGMENTS

The research leading to these results has received funding from the European Community's Seventh Framework Programme FP7/2007-2011 under grant agreement n°224042, and the DLR Project RUS 11/019 (bilateral cooperation with Russia). A. E.-M. acknowledges support from the Catalan Agència de Gestió d'Ajuts Universitaris I de Recerca (AGAUR) through grant (BE-DGR 2011, BE100777), and M. S. acknowledges support from the Federal Target Programme, Russia (contract n°16.522.11.2001) and DAAD Germany (Reg. n°10.72.2012).

## REFERENCES

- <sup>1</sup> Amman, E. O. and Yarborough, J. M., "Optical parametric oscillation in proustite," *Appl. Phys. Lett.* **17**, 233-235 (1970).
- <sup>2</sup> Hanna, D. C., Luther-Davies, B., Rutt, H. N., and Smith, R. C., "Reliable operation of a proustite parametric oscillator," *Appl. Phys. Lett.* **20**, 34-36 (1972).
- <sup>3</sup> Hanna, D. C., Luther-Davies, B., and Smith, R. C., "Singly resonant proustite parametric oscillator tuned from 1.22 to 8.5  $\mu\text{m}$ ," *Appl. Phys. Lett.* **22**, 440-442 (1973).
- <sup>4</sup> Fan, Y. X., Eckardt, R. C., Byer, R. L., Route, R. K., and Feigelson, R. S., "AgGaS<sub>2</sub> infrared parametric oscillator," *Appl. Phys. Lett.* **45**, 313-315 (1984).
- <sup>5</sup> Phua, P. B., Wu, R. F., Chong, T. C., and Xu, B. X., "Nanosecond AgGaS<sub>2</sub> optical parametric oscillator with more than 4 micron output," *Jpn. J. Appl. Phys.* **36**, L1661-L1664 (1997).
- <sup>6</sup> Allik, T. H., Chandra, S., Hovis, W. W., Simi, C. G., and Hutchinson, J. A., "Advances in optical parametric oscillators with application to remote chemical sensing," *Proc. SPIE* **3383**, 58-64 (1998).
- <sup>7</sup> Vodopyanov, K. L., Maffetone, J. P., Zwieback, I., and Rudermann, W., "AgGaS<sub>2</sub> optical parametric oscillator continuously tunable from 3.9 to 11.3  $\mu\text{m}$ ," *Appl. Phys. Lett.* **75**, 1204-1206 (1999).
- <sup>8</sup> Wang, T.-J., Kang, Z.-H., Zhang, H.-Z., He, Q.-Y., Qu, Y., Feng, Z.-S., Jiang, Y., Gao, J.-Y., Andreev, Y. M., and Lanskii, G. V., "Wide-tunable, high energy AgGaS<sub>2</sub> optical parametric oscillator," *Opt. Express* **14**, 13001-13006 (2006).
- <sup>9</sup> Wang, T.-J., Kang, Z.-H., Zhang, H.-Z., Feng, Z.-S., Jiang, Y., Gao, J.-Y., Andreev, Y. M., Lanskii, G. V., and Shaiduko, A. V., "Model and experimental investigation of frequency conversion in AgGaGe<sub>x</sub>S<sub>2(1+x)</sub> (x=0,1) crystals," *J. Phys. D: Appl. Phys.* **40**, 1357-1362 (2007).
- <sup>10</sup> Wang, T.-J., Zhang, H.-Z., Wu, F.-G., Feng, Z.-S., Zang, H.-Y., Kang, Z.-H., Jiang, Y., and Gao, J.-Y., "3-5  $\mu\text{m}$  AgGaS<sub>2</sub> optical parametric oscillator with prism cavity," *Laser Phys.* **3**, 377-380 (2009).
- <sup>11</sup> Takaoka, E. and Kato, K., "Tunable IR generation in HgGa<sub>2</sub>S<sub>4</sub>," Conference on Lasers and Electro-Optics CLEO'98, San Francisco (CA), USA, May 3-8, 1998, paper CWF39, 1998 OSA Technical Digest Series Vol. 6, pp. 253-254.
- <sup>12</sup> Kato, K. and Miyata, K., "Nd:YAG laser pumped HgGa<sub>2</sub>S<sub>4</sub> parametric oscillator," *Proc. SPIE* **8604**, 8604-1K (2013).
- <sup>13</sup> Badikov, V. V., Don, A. K., Mitin, K. V., Seregin, A. M., Sinaiskii, V. V., and Schebetova, N. I., "A HgGa<sub>2</sub>S<sub>4</sub> optical parametric oscillator," *Quantum Electron.* **33**, 831-832 (2003).

- <sup>14</sup> Badikov, V. V., Don, A. K., Mitin, K. V., Seregin, A. M., Sinaiskii, V. V., Shchebetova, N. I., and Shchetinkina, T. A., „Optical parametric mid-IR HgGa<sub>2</sub>S<sub>4</sub> oscillator pumped by a repetitively pulsed Nd:YAG laser,“ *Quantum Electron.* **37**, 363-365 (2007).
- <sup>15</sup> Tyazhev, A., Marchev, G., Badikov, V., Esteban-Martin, A., Badikov, D., Panyutin, V., Shevyrdyaeva, G., Sheina, S., Fintisova, A., and Petrov, V., “High-power HgGa<sub>2</sub>S<sub>4</sub> optical parametric oscillator pumped at 1064 nm and operating at 100 Hz,” *Las. & Phot. Rev.* **7**, L1-L4, DOI 10.1002/lpor.201300023 (2013).
- <sup>16</sup> Mangin, J., Mennerat, G., Gadret, G., Badikov, V., and de Miscault, J.-C., „Comprehensive formulation of temperature-dependent dispersion of optical materials: illustration with case of temperature tuning of a mid-IR HgGa<sub>2</sub>S<sub>4</sub> OPO,“ *J. Opt. Soc. Am. B* **26**, 1702-1709 (2009).
- <sup>17</sup> Esteban-Martin, A., Marchev, G., Badikov, V., Panyutin, V., Petrov, V., Shevyrdyaeva, G., Badikov, D., Starikova, M., Sheina, S., Fintisova, A., and Tyazhev, A., “High-energy optical parametric oscillator for the 6 μm spectral range based on HgGa<sub>2</sub>S<sub>4</sub> pumped at 1064 nm,” *Las. & Phot. Rev.* **7**(2013), submitted.
- <sup>18</sup> Badikov, V. V., Don, A. K., Mitin, K. V., Seryogin, A. M., Sinaiskiy, V. V., and Schebetova, N. I., “Optical parametric oscillator on an Hg<sub>1-x</sub>Cd<sub>x</sub>Ga<sub>2</sub>S<sub>4</sub> crystal,” *Quantum Electron.* **35**, 853-856 (2005).
- <sup>19</sup> Zondy, J.-J., Vedenyapin, V., Yelisseyev, A., Lobanov, S., Isaenko, L., and Petrov, V., “LiInSe<sub>2</sub> nanosecond optical parametric oscillator,” *Opt. Lett.* **30**, 2460-2462 (2005).
- <sup>20</sup> Marchev, G., Tyazhev, A., Vedenyapin, V., Kolker, D., Yelisseyev, A., Lobanov, S., Isaenko, L., Zondy, J.-J., and Petrov, V., “Nd:YAG pumped nanosecond optical parametric oscillator based on LiInSe<sub>2</sub> with tunability extending from 4.7 to 8.7 μm,” *Opt. Express* **17**, 13441-13446 (2009).
- <sup>21</sup> Marchev, G., Tyazhev, A., Vedenyapin, V., Kolker, D., Yelisseyev, A., Lobanov, S., Isaenko, L., Zondy, J.-J., and Petrov, V., “Broadly tunable LiInSe<sub>2</sub> optical parametric oscillator pumped by a Nd:YAG laser,” *Proc. SPIE* **7487**, 74870F/1-9 (2009).
- <sup>22</sup> Tyazhev, A., Marchev, G., Vedenyapin, V., Kolker, D., Yelisseyev, A., Lobanov, S., Isaenko, L., Zondy, J.-J., and Petrov, V., “LiInSe<sub>2</sub> nanosecond optical parametric oscillator tunable from 4.7 to 8.7 μm,” *Proc. SPIE* **7582**, 75820E/1-11 (2010).
- <sup>23</sup> Petrov, V., Schunemann, P. G., Zawilski, K. T., and Pollak, T. M., “Non-critical singly resonant OPO operation near 6.2 μm based on a CdSiP<sub>2</sub> crystal pumped at 1064 nm,” *Opt. Lett.* **34**, 2399-2401 (2009).
- <sup>24</sup> Petrov, V., Marchev, G., Schunemann, P. G., Tyazhev, A., Zawilski, K. T., and Pollak, T. M., “Subnanosecond, 1 kHz, temperature-tuned, noncritical mid-infrared optical parametric oscillator based on CdSiP<sub>2</sub> crystal pumped at 1064 nm,” *Opt. Lett.* **35**, 1230-1232 (2010).
- <sup>25</sup> Marchev, G., Pirzio, F., Agnesi, A., Reali, G., Petrov, V., Tyazhev, A., Schunemann, P. G., and Zawilski, K. T., “1064 nm pumped CdSiP<sub>2</sub> optical parametric oscillator generating sub-300 ps pulses near 6.15 μm at 1-10 kHz repetition rates,” *Opt. Commun.* **291**, 326-328 (2013).
- <sup>26</sup> Marchev, G., Tyazhev, A., Stöppler, G., Eichhorn, M., Schunemann, P., and Petrov, V., “Comparison of linear and RISTRA cavities for a 1064 nm pumped CdSiP<sub>2</sub> OPO,” *Proc. SPIE* **8240**, 82400E/1-7 (2012).
- <sup>27</sup> Tyazhev, A., Vedenyapin, V., Marchev, G., Isaenko, L., Kolker, D., Lobanov, S., Petrov, V., Yelisseyev, A., Starikova, M., and Zondy, J.-J., “Singly-resonant optical parametric oscillation based on the wide band-gap mid-IR nonlinear optical crystal LiGaS<sub>2</sub>,” *Opt. Mater.* **35**, 1612-1615 (2013).
- <sup>28</sup> Tyazhev, A., Kolker, D., Marchev, G., Badikov, V., Badikov, D., Shevyrdyaeva, G., Panyutin, V., and Petrov, V., “Midinfrared optical parametric oscillator based on the wide-bandgap BaGa<sub>4</sub>S<sub>7</sub> nonlinear crystal,” *Opt. Lett.* **37**, 4146-4148 (2012).
- <sup>29</sup> Jackson, A. G., Ohmer, M. C., and LeClair, S. R., “Relationship of the second order nonlinear optical coefficient to energy gap in inorganic non-centrosymmetric crystals,” *Infrared Phys. Technol.* **38**, 233-244 (1997).
- <sup>30</sup> Andreev, Yu. M., Badikov, V. V., Voevodin, V. G., Geiko, L. G., Geiko, P. P., Ivashchenko, M. V., Karapuzikov, A. I., and Sherstov, I. V., „Radiation resistance of nonlinear crystals at a wavelength of 9.55 μm,“ *Quantum Electron.* **31**, 1075-1078 (2001).

- <sup>31</sup> Petrov, V., Badikov, V., and Panyutin, V., "Quaternary nonlinear optical crystals for the mid-infrared spectral range from 5 to 12 micron," In: *Mid-Infrared Coherent Sources and Applications*, ed. by M. Ebrahim-Zadeh and I. Sorokina, *NATO Science for Peace and Security Series - B: Physics and Biophysics*, Springer (2008), pp. 105-147.
- <sup>32</sup> ISO 11254-2, 2001, Lasers and laser-related equipment - Determination of laser-induced damage threshold of optical surfaces – Part 1: 1-on-1 test, and Part 2: S-on-1 test.
- <sup>33</sup> Zawilski, K. T., Setzler, S. D., Schunemann, and Pollak, T. M., „Increasing the laser-induced damage threshold of single-crystal ZnGeP<sub>2</sub>,“ *J. Opt. Soc. Am. B* **23**, 2310-2316 (2006).
- <sup>34</sup> Peterson, R. D., Schepler, K. L., Brown, J. L., and Schunemann, P. G., „Damage properties of ZnGeP<sub>2</sub> at 2 μm,“ *J. Opt. Soc. Am. B* **12**, 2142-2146 (1995).
- <sup>35</sup> Badikov, V. V., Kuzmin, N. V., Laptev, V. B., Malinovsky, A. L., Mitin, K. V., Nazarov, G. S., Ryabov, E. A., Seryogin, A. M., Schebetova, N. I., „A study of the optical and thermal properties of nonlinear mercury thiogallate crystals,“ *Quantum Electron.* **34**, 451-456 (2004).
- <sup>36</sup> Yao, J., Yin, W., Feng, K., Li, X., Mei, D., Lu, Q., Ni, Y., Zhang, Z., Hu, Z., and Wu, Y., „Growth and characterization of BaGa<sub>4</sub>Se<sub>7</sub> crystal,“ *J. Cryst. Growth* **346**, 1-4 (2012).
- <sup>37</sup> Marchev, G., Tyazhev, A., Petrov, V., Schunemann, P. G., Zawilski, K. T., Stöppler, G., and Eichhorn, M., “Optical parametric generation in CdSiP<sub>2</sub> at 6.125 μm pumped by 8 ns long pulses at 1064 nm,” *Opt. Lett.* **37**, 740-742 (2012).
- <sup>38</sup> Stoeppler, G., Schellhorn, M., and Eichhorn, M., “Enhanced beam quality for medical applications at 6.45 μm by using a RISTRA ZGP OPO,” *Laser Phys.* **22**, 1095-1098 (2012).
- <sup>39</sup> Chuchumishev, D., Gaydardzhiev, A., Trifonov, A., and Buchvarov, I., “Single-frequency MOPA system with near-diffraction-limited beam quality,“ *Quantum Electron.* **42**, 528-530 (2012).